Raman scattering from a Bose condensate

Jesús Martínez-Linares[1] and G. S. Agarwal[1,2]
[1]*Max-Planck-Institut für Quantenoptik, Hans-Kopfermann-Strasse 1, D-85748 Garching, Germany*
[2]*Physical Research Laboratory, Ahmedabad 380 009, India*
(Received 17 September 1997)

We calculate Raman scattering of light from a Bose condensate of dilute gas confined in a harmonic trap. We examine the changes in the Raman line shape as a function of temperature. The linewidth exhibits a remarkable transition as the system is cooled down from the noncondensed to the condensed phase. We also present results for sidebands arising from deeper traps. We show that all these results on Raman line shapes are especially pronounced in the backward direction.
[S1050-2947(98)00304-7]

PACS number(s): 03.75.Fi, 05.30.Jp, 42.65.An, 42.50.Vk

I. INTRODUCTION

Bose-Einstein condensation of low-density atomic vapors is now well demonstrated [1]. Optical spectroscopy methods [2] are of prime interest in the analysis of the properties of the condensate. As is well known, Raman spectroscopy has been an important tool for studying the properties of atomic systems. Raman spectroscopy is also known to be especially useful for the study of systems undergoing phase transitions. Thus one would think of Raman scattering as especially suited for studying the characteristics of Bose condensates formed from weakly interacting atoms. In particular, the nature of the transition can be explored as one goes from the noncondensed phase to the condensed phase. With this in mind, we calculate the line shape for Raman scattering as a function of the transition temperature. We demonstrate distinct changes in the linewidth as we change the temperature from above to below the critical temperature. We find that the line shapes are also quite sensitive to the direction of propagation of the pump and Stokes fields. We also examine the nature of the sidebands in Raman scattering for deeper sidebands.

The trap potential is included in our treatment; however, we treat only the case of noninteracting atoms. An exact numerical treatment is incorporated in order to take into account finite-size effects steaming from the finite number of trapped atoms.

This paper is organized as follows. In Sec. II the magneto-optical harmonic trap and the Hamiltonian governing the dynamics of the trapped atoms interacting with photons are reviewed. Section III is devoted to the calculation of Raman transition amplitudes for the confined atoms. The results are discussed in Sec. IV. We end with conclusions and a summary of the results in Sec. V.

II. HAMILTONIAN FORMALISM

Energy levels of alkali-metal atoms undergo Zeeman splitting when exposed to an external magnetic field $\vec{B}$. Depending on the sign of the magnetic sublevel, the atom will experience an attractive or repulsive force that tends to confine it in the local minima of $\vec{B}$. Typically, in a magneto-optical trap (MOT) [3], the magnetic field is designed to form an effective potential that can be well approximated by a harmonic-oscillator potential at the bottom of the trap.

We briefly described the tools used in the calculation of the quantum statistics of the trapped gas. The distribution of the atoms in the states of the trap is given by the Bose-Einstein statistics

$$N_{\vec{l},g}=(\lambda^{-1}e^{\beta E'_{\vec{l}}}-1)^{-1}, \tag{1}$$

where $\beta=1/k_BT$, $E'_{\vec{l}}=E_{\vec{l}}-E_0$ are the eigenenergies of the harmonic-oscillator trap once the ground-state energy has been substracted, and λ is the fugacity. λ can be calculated through the normalization condition

$$N=\sum_{\vec{l}} N_{\vec{l},g}, \tag{2}$$

where N is the total number of particles in the trap. An analytical approximation can be obtained for this summation [4] as

$$N=N_0+\left(\frac{k_BT}{\hbar\nu}\right)^3 g_3(\lambda)+\gamma\left(\frac{k_BT}{\hbar\nu}\right)^2 g_2(\lambda). \tag{3}$$

Here ν is the frequency of the harmonic trap, $\gamma=1.5$ for an isotropic trap, $g_i(\lambda)=\Sigma_n\lambda^n/n^i$ are polylogarithmic functions, and N_0 is the number of particles in the ground state of the trap. From Eq. (1) one can readily see that the fugacity satisfies the relation

$$N_0=\frac{\lambda}{1-\lambda}, \tag{4}$$

so that $0\leqslant\lambda<1$. The fugacity and its polylogarithmic functions increase monotonically as we cool down the gas. Since $g_i(\lambda)$ are bounded by $g_i(1)$, Eq. (3) can only be satisfied at low temperature at the expense of populating the ground state, originating the condensed phase. The critical temperature T_c at which $g_i(\lambda)$ saturates can be estimated by imposing $N_0=0$ in Eq. (3) for $\lambda=1$. One gets

$$T_c=\frac{\hbar\nu}{k_B}\left[\frac{N}{\xi(3)}\right]^{1/3}\left\{1-\frac{\gamma\xi(2)}{3\xi(3)^{2/3}}\frac{1}{N^{1/3}}\right\}, \tag{5}$$

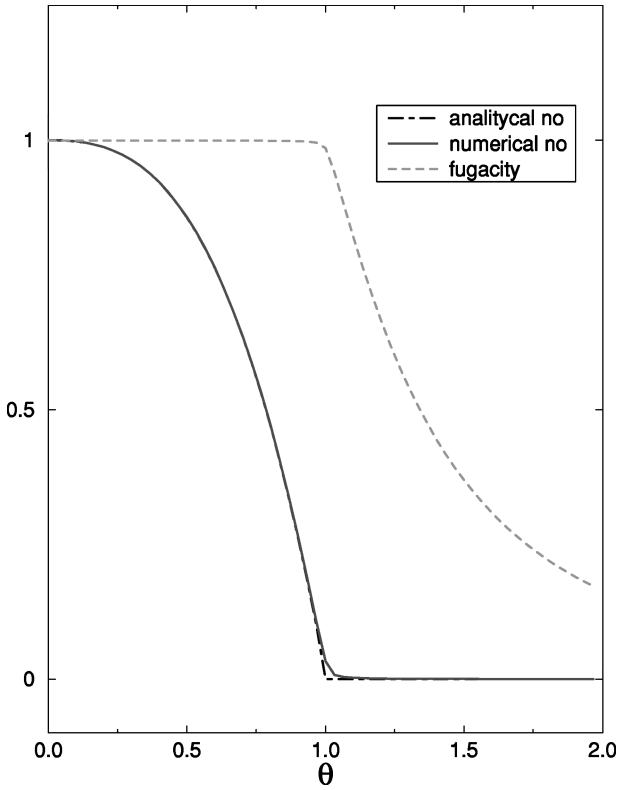

FIG. 1. Temperature dependence of the fugacity (dashed line) and of the fraction of atoms in the condensate. The solid line gives the exact (numerical) calculation and the dot-dashed line the analytical approximation derived by Grossman. Small finite-size effects ($N_T=2000$) can be appreciated around the critical temperature.

where $\xi(i)\equiv g_i(1)$.

As we cool the system below this critical temperature the fraction of particles in the condensate increases until all particles occupy the condensate at $T=0$. This can be seen in Fig. 1, where the Bose-condensate fractions $n_0=N_0/N$ calculated numerically after Eq. (2) (solid line) and according to the analytical expression (3) (dot-dashed line) are plotted as a function of the normalized temperature $\theta=T/T_c$. We have considered an isotropical trap with $N=2000$. Finite-size effects can be appreciated around the critical temperature. The numerically calculated fugacity is also plotted in Fig. 1, showing an asymptotical approach to unity in the condensation regime $\theta<1$.

Let us now describe the tools used to model the Raman optical response of the gas. We start from the quantum field theory of trapped atoms interacting with photons developed by Lewenstein *et al.* [5]. We restrict the discussion to the following approximations [6]: the three-level atom approximation, in which a Hilbert space expanded by three states $\{|g\rangle,|e\rangle,|f\rangle\}$ suffices to describe the atomic electronic structure; the rotating-wave approximation, in which we pick out only the terms of the interaction Hamiltonian that conserve the number of excitations; the atom-field interaction in the dipole approximation, in which the resonant wavelength $\lambda\!\!\!^{-}_L$ is much larger than the typical atomic size a_0, and the ideal gas approximations, in which the density of the gas n is low enough to neglect atom-atom interactions (this condition requires $na_0^3\ll 1$). This allow us to use bare photons and excited atoms as good elementary excitations inside a Bose-condensed gas, so we can neglect collective optical excitations. This is justified under the condition $n\lambda\!\!\!^{-3}_L\ll 1$.

The second quantized form of the Hamiltonian governing the system can be obtained by taking the expectation value of the particle Hamiltonian with respect to the quantum fields $\Psi(\vec{r})$ satisfying the bosonic commutation relation

$$[\Psi(\vec{r}),\Psi^\dagger(\vec{r}')]=\delta(\vec{r}-\vec{r}'). \tag{6}$$

Here $\vec{r}$ is the coordinate vector of the center of mass of the atom in the trap, so $n(\vec{r})=\Psi^\dagger(\vec{r})\Psi(\vec{r})$ represents the density operator of particles associated with the quantum field.

We express the field operators in the Fock representation, i.e., in terms of operators that describe the degree of occupation of the state in the base given by the eigenstates of the bare Hamiltonian. This Hamiltonian corresponds to the states of a three-dimensional harmonic-oscillator potential. Therefore, we introduce the operators $\{g_{\vec{l}},g_{\vec{l}}^\dagger\}$ that anihilate or create atoms in the $\vec{l}$ state of the ground-state potential, $\{e_{\vec{m}},e_{\vec{m}}^\dagger\}$, which play the same role for the $\vec{m}$ intermediate Raman states, and $\{f_{\vec{p}},f_{\vec{p}}^\dagger\}$, which describe the vibrational structure of the final state.

The occupation number operators fulfill the standard commutation relations for bosonic atoms:

$$[g_{\vec{l}},g_{\vec{l}'}^\dagger]=\delta_{\vec{l}\,\vec{l}'},\quad [e_{\vec{m}},e_{\vec{m}'}^\dagger]=\delta_{\vec{m}\vec{m}'},\quad [f_{\vec{p}},f_{\vec{p}'}^\dagger]=\delta_{\vec{p}\vec{p}'}. \tag{7}$$

In this representation the field operators reads

$$\Psi^g(\vec{r})=\sum_{\vec{l}}\ g_{\vec{l}}\ \phi_{\vec{l}}^g(\vec{r}),$$

$$\Psi^e(\vec{r})=\sum_{\vec{m}}\ e_{\vec{m}}\phi_{\vec{m}}^e(\vec{r}),$$

$$\Psi^f(\vec{r})=\sum_{\vec{p}}\ f_{\vec{p}}\ \phi_{\vec{p}}^f(\vec{r}), \tag{8}$$

where the coefficients are given by the three-dimensional harmonic-oscillator eigenstates. For instance, for an isotropic trap

$$\phi_{\vec{l}}^g(\vec{r})\equiv\langle\vec{r}|\vec{l},g\rangle=\phi_{l_x}^g(x)\phi_{l_y}^g(y)\phi_{l_z}^g(z),$$

$$\phi_l(z)=\frac{1}{\sqrt{a_b\sqrt{2\pi}2^l l!}}H_l\left(\frac{z}{\sqrt{2}a_b}\right)\exp\left(-\frac{z^2}{4a_b^2}\right), \tag{9}$$

where H_l are Hermite polynomials and $a_b=\sqrt{\hbar/2m\nu}$ is the size of the bare ground-state wave function determined by the atomic mass m and the frequency of the trap ν.

Within the approximations given before, the Hamiltonian of the system in the Fock representation becomes

$$\mathcal{H}=\mathcal{H}_0+\mathcal{H}_f+\mathcal{H}_{af}+\mathcal{H}_{a\alpha}, \tag{10}$$

where the bare atomic Hamiltonian reads

$$\mathcal{H}_0=\sum_{\vec{l}}\hbar w_{\vec{l}}^{g} g_{\vec{l}}^{\dagger} g_{\vec{l}}+\sum_{\vec{m}}\hbar(w_{\vec{m}}^{e}+w_0)e_{\vec{m}}^{\dagger}e_{\vec{m}}$$

$$+\sum_{\vec{p}}\hbar(w_{\vec{p}}^{f}+w_f)f_{\vec{p}}^{\dagger}f_{\vec{p}}. \tag{11}$$

Here $w_{\vec{l}}^{g}$, $w_{\vec{m}}^{e}$, and $w_{\vec{p}}^{f}$ are the eigenfrequencies of the center-of-mass motion of the atoms corresponding to the $|g\rangle$, $|e\rangle$, and $|f\rangle$ electronic states, namely,

$$w_{\vec{l}}^{g}=\nu\{l_x+l_y+l_z+3/2\},$$

$$w_{\vec{m}}^{e}=\nu\{m_x+m_y+m_z+3/2\},$$

$$w_{\vec{p}}^{f}=\nu\{p_x+p_y+p_z+3/2\}. \tag{12}$$

Note that the energy differences $\hbar w_0$ and $\hbar w_f$, corresponding, respectively, to the electronic transition from the ground state $|g\rangle$ to the intermediate Raman state $|e\rangle$ and to the final state $|f\rangle$, have been written down explicitly in Eq. (11).

The Hamiltonian for the free electromagnetic (em) field is

$$\mathcal{H}_f=\sum_{\mu}\int d\vec{k}\hbar ck a_{\vec{k},\mu}^{\dagger}a_{\vec{k},\mu}, \tag{13}$$

where $a_{\vec{k},\mu}, a_{\vec{k},\mu}^{\dagger}$ are anihilation and creation operators of photons of momentum $\vec{k}$ and linear polarization $\vec{\varepsilon}_{\vec{k},\mu}$. A summation over the polarization $\mu=1,2$ states has to be done in order to account for all possible transitions in the Zeeman multiplet.

$\mathcal{H}_{af}$ characterizes the interaction between the atom and the vacuum modes of the em field. For instance, for the $|e\rangle \rightarrow |g\rangle$ transition it reads

$$\mathcal{H}_{af}=\frac{i\hbar}{\sqrt{2\epsilon_0(2\pi)^3}}\sum_{\mu}\sum_{\vec{l},\vec{m}}\int d^3\vec{k}\sqrt{k}(\vec{d}\cdot\vec{\varepsilon}_{\vec{k},\mu})$$
$$\times\mathcal{F}_{\vec{l}\vec{m}}(\vec{k})a_{\vec{k},\mu}^{\dagger}g_{\vec{l}}^{\dagger}e_{\vec{m}}+\text{H.c.} \tag{14}$$

Here $\vec{d}$ is the dipole moment of the electronic transition. The conservation of momentum is expressed by the Franck-Condon matrix elements

$$\mathcal{F}_{\vec{l}\vec{m}}(\vec{k})=\langle\vec{l}|e^{-i\vec{k}\cdot\vec{r}}|\vec{m}\rangle. \tag{15}$$

$|\mathcal{F}_{ml}(-k)|^2$ is proportional to the probability that an atom will make the transition from $|m,e\rangle$ to $|l,g\rangle$ by emitting a photon of frequency $ck_0+\nu(m-l)$ with any polarization.

Finally, the interaction between the atomic dipole of the atom characterized by the dipole moment operator

$$\vec{p}(\vec{r})=\vec{d}_{eg}^{*}\Psi_e^{\dagger}(\vec{r})\Psi_g(\vec{r})+\vec{d}_{ef}^{*}\Psi_e^{\dagger}(\vec{r})\Psi_f(\vec{r})+\text{H.c.}$$

$$=\vec{d}_{eg}^{*}\sum_{\vec{l},\vec{m}}e_{\vec{m}}^{\dagger}g_{\vec{l}}\phi_{\vec{m}}^{e*}(\vec{r})\phi_{\vec{l}}^{g}(\vec{r})+\vec{d}_{ef}^{*}\sum_{\vec{p},\vec{m}}e_{\vec{m}}^{\dagger}f_{\vec{p}}\phi_{\vec{m}}^{e*}(\vec{r})\phi_{\vec{p}}^{f}(\vec{r})$$
$$+\text{H.c.} \tag{16}$$

and the laser fields

$$\vec{E}_{\alpha}(\vec{r},t)=\vec{\epsilon}_{\alpha}e^{i(\vec{k}_{\alpha}\vec{r}-\omega_{\alpha}t)}+\text{c.c.},\quad \alpha=L,S, \tag{17}$$

is determined by the interaction Hamiltonian in the dipole approximation

$$\mathcal{H}_{a\alpha}=-\int d\vec{r}\,\vec{p}(\vec{r})\cdot\vec{E}_{\alpha}(\vec{r},t). \tag{18}$$

Here $\alpha=L,S$ stands for the pump and Stokes field, respectively. Converting to the Fock representation given in Eqs. (8), we find the second quantized form of the Hamiltonian to be

$$\mathcal{H}_{aL}=-d^{*}\epsilon_L e^{-iw_Lt}\sum_{\vec{l},\vec{m}}\mathcal{F}_{\vec{m}\vec{l}}(-\vec{k}_L)e_{\vec{m}}^{\dagger}g_{\vec{l}}+\text{H.c.},$$

$$\mathcal{H}_{aS}=-d^{*}\epsilon_S e^{-iw_St}\sum_{\vec{p},\vec{m}}\mathcal{F}_{\vec{m}\vec{p}}(-\vec{k}_S)e_{\vec{m}}^{\dagger}f_{\vec{p}}+\text{H.c.} \tag{19}$$

Usual parity selection rules are exhibited by the dipole moment matrix elements appearing in the prefactor of the interaction Hamiltonians (19), as stated by the Wigner-Eckart theorem [7]. On the other hand, the quantization of the atomic center-of-mass motion reveals itself in the Franck-Condon factors entering the expression of the Hamiltonian. As will be stressed in Sec. IV, additional selection rules between vibrational levels can be brought about by the oscillatory behavior of the Franck-Condon factors.

III. RAMAN SCATTERING FROM A MOT

In this section we calculate the transition probability per unit time $\mathcal{W}_R$ for the scattering of light from a confined gas exposed to two weak fields of frequencies w_S and w_L. This rate can be derived from the general expression for radiative transition rates carried in second-order time-dependent perturbation theory [8]. We obtain

$$\mathcal{W}_R^{(\vec{l}\rightarrow\vec{p})}=\frac{2\pi}{\hbar^2}\left|\sum_{m}\frac{\langle f,\vec{p}|\mathcal{H}_I^{S}|e,\vec{m}\rangle\langle e,\vec{m}|\mathcal{H}_I^{L}|g,\vec{l}\rangle}{\hbar w_0+\hbar w_{\vec{m}\vec{l}}-\hbar w_L}\right|^2$$
$$\times\delta(w_f-(w_L-w_S)+w_{\vec{p}\vec{l}}), \tag{20}$$

where the vibrational transition energies are

$$w_{\vec{m}\vec{l}}=\nu\{(m_x-l_x)+(m_y-l_y)+(m_z-l_z)\}. \tag{21}$$

The Dirac δ in Eq. (20) ensures conservation of energy in the transition from the initial $|g,l\rangle$ state to the final $|f,p\rangle$ state. $\mathcal{H}_I^{(S,L)}$ are the interaction Hamiltonians for these stimulated Raman transitions.

The matrix elements appearing in Eq. (20) can be readily calculated after Eq. (19) to yield

$$\langle f,\vec{p}|\mathcal{H}_I^{S}|e,\vec{m}\rangle\langle e,\vec{m}|\mathcal{H}_I^{L}|g,\vec{l}\rangle=[\mathcal{F}_{\vec{m}\vec{l}}(-\vec{k}_L)d_{eg}\epsilon_L]$$
$$\times[\mathcal{F}_{\vec{p}\vec{m}}(\vec{k_S})d_{fe}\epsilon_S^{*}]. \tag{22}$$

In the large detuning regime $\Delta\gg\nu$ ($\Delta\equiv w_0-w_L$), the denominator in Eq. (20) can be approximated by $\hbar\Delta$. The summation over intermediate vibrational states can now be performed with the help of the closure relation, namely,

$$\sum_{\vec{m}} \mathcal{F}_{\vec{p}\vec{m}}(\vec{k}_S)\mathcal{F}_{\vec{m}\vec{l}}(-\vec{k}_L) = \sum_{\vec{m}} \langle \vec{p},g|e^{i\vec{k}_S\cdot\vec{r}}|\vec{m},e\rangle \times \langle \vec{m},e|e^{-i\vec{k}_L\cdot\vec{r}}|\vec{l},g\rangle = \mathcal{F}_{\vec{p}\vec{l}}(\vec{k}_S-\vec{k}_L). \quad (23)$$

On the other hand, we can take into account the incoherent effects by means of replacing the Dirac δ function by a Lorentzian characterized by the half-width Γ, i.e.,

$$\delta(w_f-(w_L-w_S)+w_{\vec{p}\vec{l}}) \rightarrow \left(\frac{1}{\pi}\right)\frac{\Gamma}{\Gamma^2+\{w_f-w_L+w_S+w_{\vec{p}\vec{l}}\}^2}. \quad (24)$$

Thus Γ is the width of the Raman line for a single atom in a trap. After all of these considerations, we can approximate the total transition rate by the expression

$$\overline{\mathcal{W}}_R \equiv \mathcal{K}^{-1}\sum_{\vec{l},\vec{p}} \mathcal{W}_R^{(\vec{l}\rightarrow\vec{p})} = \sum_{\vec{l},\ \vec{p}} \frac{N^0_{\vec{l},g}|\mathcal{F}_{\vec{p}\vec{l}}(\vec{k}_S-\vec{k}_L)|^2}{\Gamma^2+\{\delta+w_{\vec{p}\vec{l}}\}^2}, \quad (25)$$

where have taken the normalization $\overline{\mathcal{W}}_R=\mathcal{W}_R/\mathcal{K}$, with

$$\mathcal{K}^{-1}=\left(\frac{d_{eg}d_{fe}\epsilon_L\epsilon_S^*}{\hbar^2\Delta}\right)^2\frac{\Gamma}{\pi}, \quad (26)$$

and we have defined the Raman detuning $\delta=w_f-w_L+w_S$. $N_{l,g}$ is the number of particle distribution in the initial state given by Eq. (1).

Choosing as the $\hat{z}$ direction the one given by $\vec{k}_S-\vec{k}_L$, the Lamb-Dicke parameter η is defined by the relation

$$a_b(\vec{k}_S-\vec{k}_L)=\eta\hat{z}. \quad (27)$$

Because of momentum conservation, the light can only excite vibrational states in the direction of the vector $\vec{k}_S-\vec{k}_L$. This fact is expressed by the factorization property of the Franck-Condon factors

$$\mathcal{F}_{\vec{p}\vec{l}}(\vec{k}_S-\vec{k}_L)=\delta_{p_xl_x}\delta_{p_yl_y}\mathcal{F}_{p_zl_z}(\eta), \quad (28)$$

reducing Eq. (25) to the expression

$$\overline{\mathcal{W}}_R=\sum_{\vec{l},p_z}\frac{N^0_{\vec{l},g}|\mathcal{F}_{p_zl_z}(\eta)|^2}{\Gamma^2+\{\delta+\nu(p_z-l_z)\}^2}. \quad (29)$$

Furthermore, the Franck-Condon factors can be calculated in closed form as

$$|\mathcal{F}_{ml}(-\eta)|^2=\eta^{2(m-l)}e^{-\eta^2}\frac{l!}{m!}[L_l^{m-l}(\eta^2)]^2, \quad (30)$$

where L_l^{m-l} are associated Laguerre polynomials. Equation (29), together with Eq. (30), is our central result for the line shape of the Raman scattering of light from a MOT.

IV. RAMAN SCATTERING FROM A CONDENSATE

The quantization of the c.m. motion of the atoms leads to a vibrational structure of the spectrum of the scattered light given in Eq. (29). The line shape of the scattered light is mainly determined by the Franck-Condon Factor between vibrational transitions. In order to see this, first consider the Lamb-Dicke limit $\eta\rightarrow 0$. In this case Eq. (29) reduces to the expression

$$\overline{\mathcal{W}}_R=\frac{N}{\Gamma^2+\delta^2}, \quad (31)$$

where we have used the normalization condition (2). In this limit the line shape does not contain any information concerning the energy distribution of the gas since the light cannot resolve the momentum distribution of the trap. A case where η will be close to zero corresponds to copropagating pump and Stokes fields so that $\vec{k}_L-\vec{k}_S=(w_L-w_S)/c\hat{z}$ and thus η will be proportional to $1-(w_S/w_L)$, which in many typical cases is close to zero.

For a small Lamb-Dicke parameter, we can perform a series expansion of the Franck-Condon factors in the form

$$\mathcal{F}_{pl}(-\eta)=\delta_{p,l}+i\eta\{\sqrt{l}\ \delta_{p,l-1}+\sqrt{l+1}\ \delta_{p,l+1}\}+O(\overline{k}_L^2). \quad (32)$$

In the limit case $\eta=0$ no c.m. transitions are allowed. The first-order correction in η in Eq. (32) introduces contributions from one-level c.m. transitions. As the Lamb-Dicke parameter η increases (going to a deeper trap or changing the direction of the Raman fields), the spatial structure of the states of the trap gets resolved, as seen in Eq. (30). The zeros of the Laguerre polynomials (30) can be viewed as expressions of destructive quantum interference between the differ-

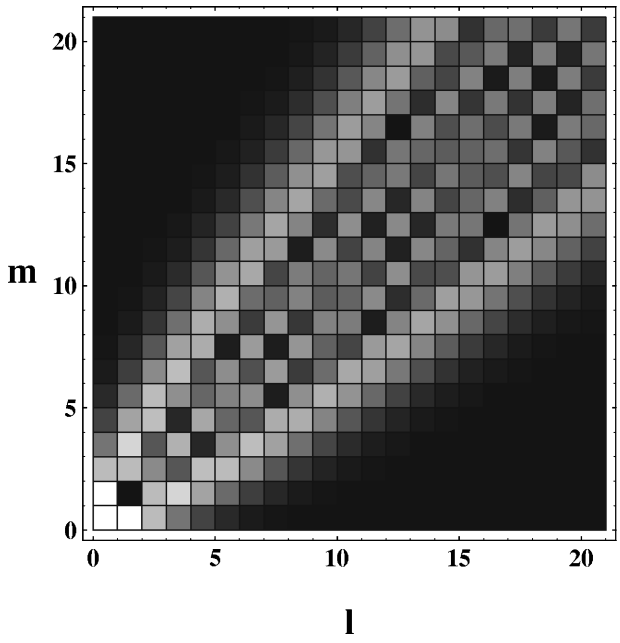

FIG. 2. Density plot of the Franck-Condon factors for transitions between different (m,l) vibrational states for $\eta=1$. The gray level covers from black to white the numerical interval $[0,e^{-1}\approx 0.37]$.

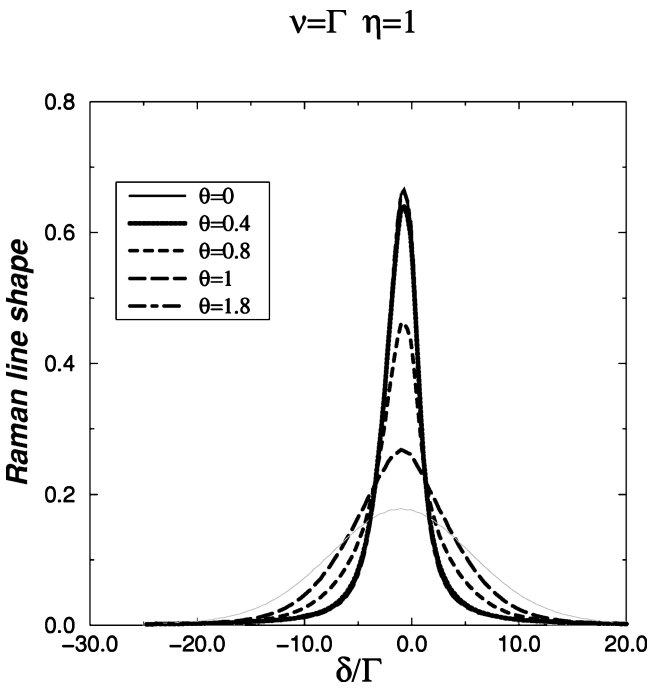

FIG. 3. Temperature dependence of the normalized Raman line shape of the scattered light given in Eq. (29) for $\nu/\Gamma=1$ and $\eta=1$. The curves are plotted for $\theta=0,\ 0.4,\ 0.8,\ 1$, and 1.8, respectively.

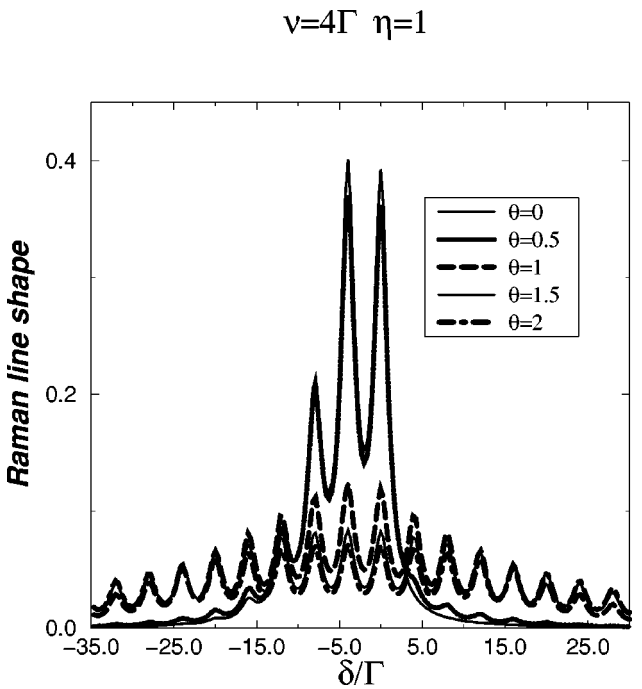

FIG. 5. Temperature dependence of the line shape of the scattered light for $\nu/\Gamma=4$ and $\eta=1$. The curves are plotted for $\theta=0,\ 0.5,\ 1,\ 1.5$, and 2, respectively.

ent nonlinear processes appearing in Eq. (32) corresponding to the transition $|l,g\rangle\rightarrow|p,f\rangle$. This is illustrated in Fig. 2, where the density plot, of the Franck-Condon factors corresponding to $\eta=1$ is shown. As can be seen in this plot, the Franck-Condon factor for the transition starting from the ground state does not oscillate. In contrast to this, the Franck-Condon factors from transitions starting from any other state l oscillate. As a matter of fact, even forbidden transitions corresponding to nodes of the Franck-Condon factors can be appreciated in Fig. 2 (black-ruled squares). This behavior allows the Bose condensate to manifest itself in the line shape, even for relatively small $\eta\approx1$, as we proceed to show now.

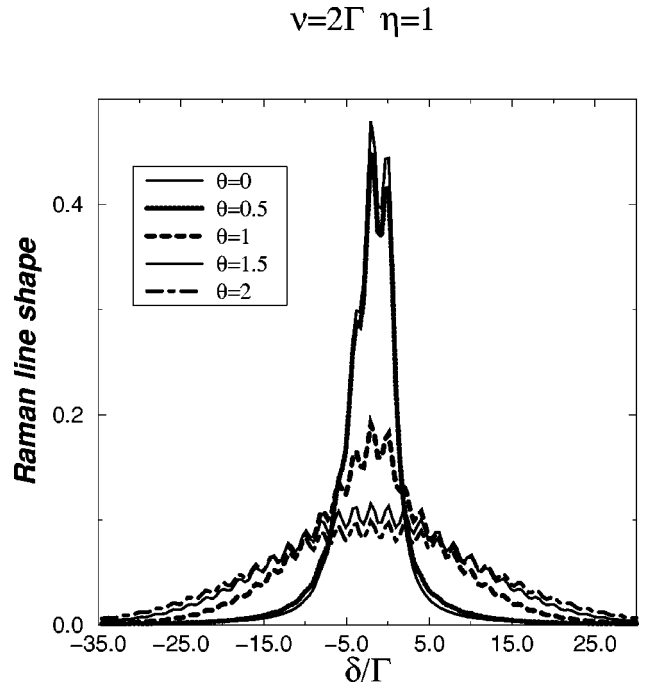

FIG. 4. Temperature dependence of the line shape of the scattered light for $\nu/\Gamma=2$ and $\eta=1$. The curves are plotted for $\theta=0,\ 0.5,\ 1,\ 1.5$, and 2, respectively.

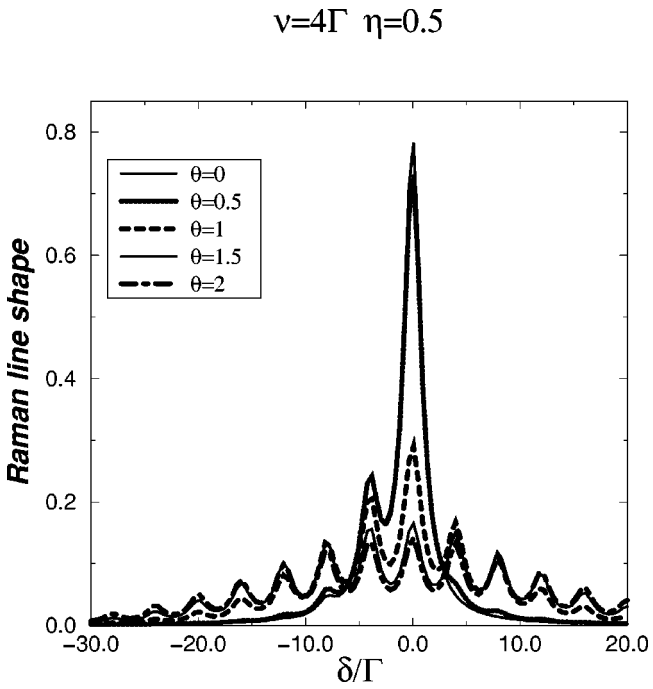

FIG. 6. Temperature dependence of the line shape of the scattered light for $\nu/\Gamma=4$ and $\eta=0.5$. The curves are plotted for $\theta=0,\ 0.5,\ 1,\ 1.5$, and 2, respectively.

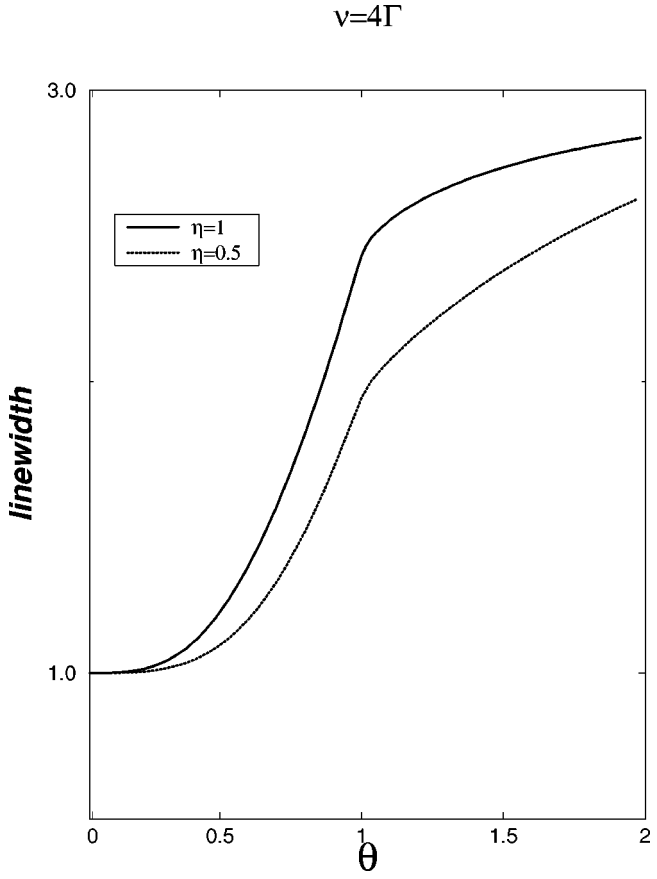

FIG. 7. Temperature dependence of the Raman linewidth of the scattered light for $\nu/\Gamma=4$ and $\eta=1$ (solid line) and $\eta=0.5$ (dashed line). The curves are normalized to the linewidth at zero temperature. The linewidth is defined in Eq. (34).

First consider the case of broad transitions in which the vibrational sideband structure cannot be resolved since it is eradicated by Γ. This case is illustrated in Fig. 3, where the lineshape (29) is plotted for $\nu/\Gamma=1$ at several temperatures. It can be seen in the plot that the line width exhibits a remarkable transition as the system is cooled down from the noncondensed to the condensed phase. The Franck-Condon factors also reveal themselves by the displacement of the peak of the line shape.

The sideband structure arises in the line shape as we increase the parameter ν/Γ. This can be appreciated in Fig. 4, where the line shape is plotted for $\nu/\Gamma=2$. A well-defined sideband structure is already present at $\nu/\Gamma=4$, as exhibited in Figs. 5 and 6, where the line shapes for $\eta=1$ and $\eta=0.5$ are plotted respectively. It can be seen by a comparison of the two plots that the intensity of the Franck-Condon factors clearly determines the peak of the sidebands in the condensate phase. Above the critical temperature, the oscillation of the Franck-Condon factors leads to a very broad Raman response when averaged over the occupation state distribution. On the other hand, these oscillations do not appear for the condensate, allowing a strong Raman response to build up. This effect can be appreciated in Fig. 7, where the temperature dependence of the linewidth defined below is shown for $\eta=1$ (solid line) and $\eta=0.5$ (dashed line). A strong narrowing of the line is apparent as we cool down over the condensate phase. The change of the linewidth around the critical temperature is stronger as η increases. It is worth remarking that in order to account for sidebands we calculated the total normalized linewidth in terms of the dispersion of the line shape, i.e.,

$$\bar{\sigma}=\frac{\sigma}{\sigma|_{\theta=0}}, \tag{33}$$

where

$$\sigma=\sqrt{\langle\delta^2\rangle-\langle\delta\rangle^2}. \tag{34}$$

V. SUMMARY

Our analysis has established the strong dependence of Raman scattering on the parameter η. For oppositely directed waves $\vec{k}_L=-\vec{k}_S$, η will be proportional to $1+(w_S/w_L)$ and could thus be large, depending on the relative size between the wavelength and the trap dimension a_b. For a fixed value of a_b, η will also change over a range of values depending on the relatives directions of the wave vectors $\vec{k}_L$ and $\vec{k}_S$. Note further that in spontaneous Raman scattering, $\vec{k}_S$ will correspond to the direction in which scattered radiation is observed. It is thus clear that the observed spectra are very sensitive to the direction of observation in the case of spontaneous Raman scattering or to the direction of the Stokes field in the case of stimulated Raman scattering. Thus the comparison between Eq. (31), which would apply to the forward scattering, and Fig. 3 shows the important differences that one will see in forward and backward scattering. The sidebands arising from deeper traps will also be observable in backward scattering.

ACKNOWLEDGMENTS

G.S.A. thanks Herbert Walther for hospitality at the Max-Planck-Institut für Quantenoptik. J.M.-L thanks Pierre Meystre for his encouraging and constructive comments and the Max-Planck-Gesellschaft (Quantenoptik) for support. J.M.-L. was also supported by the TMR Program under Contract No. ERBFMBICT950426.

[1] M. H. Anderson, J. R. Ensher, M. R. Matthews, C. E. Wieman, and E. A. Cornell, Science **269**, 198 (1995); C. C. Bradley, C. A. Sackett, J. J. Tollett, and R. G. Hulet, Phys. Rev. Lett. **75**, 1687 (1995); K. B. Davis, M.-O. Mewes, M. R. Andrews, N. J. van Druten, D. S. Kurn, and W. Ketterle, *ibid.* **75**, 3969 (1995).

[2] B. V. Svistunov and G. V. Shlyapnikov, Zh. Éksp. Teor. Fiz. **97**, 821 (1990) [Sov. Phys. JETP **70**, 460 (1990)]; H. D.

Politzer, Phys. Rev. A **43**, 6444 (1991); J. Javanainen, Phys. Rev. Lett. **72**, 2375 (1994); L. You, M. Lewenstein, and J. Cooper, Phys. Rev. A **50**, R3565 (1994); J. Javanainen, Phys. Rev. Lett. **75**, 1927 (1995); O. Morice, Y. Castin, and J. Dalibard, Phys. Rev. A **51**, 3896 (1995); A. Csordas, R. Graham, and P. Szepfalusy, *ibid.* **54**, R2543 (1996).

[3] C. Monroe, W. Swann, H. Robinson, and C. Wieman, Phys. Rev. Lett. **65**, 1571 (1990); C. Monroe, E. A. Cornell, C. A. Sackett, C. J. Myatt, and C. Wieman, *ibid.* **70**, 414 (1993).

[4] S. Grossmann and M. Holthaus, Z. Naturforsch. Teil A **50A**, 921 (1995).

[5] M. Lewenstein, L. You, J. Cooper, and K. Burnett, Phys. Rev. A **50**, 2207 (1994).

[6] See, for instance, J. I. Cirac, M. Lewenstein, and P. Zoller, Phys. Rev. A **50**, 3409 (1994).

[7] Popularly $\vec{d}_{eg}=[3j]\langle J_e|\vec{d}|J_g\rangle$. See B. W. Shore, *The Theory of Coherent Atomic Excitation* (Wiley, New York, 1990), Vol. II, pp. 1429–1436.

[8] See, for example, R. Loudon, *The Quantum Theory of Light* (Oxford University Press, London, 1983), p. 195.